SMEARED-CRACK MODELING OF CONCRETE TENSION SPLITTING

By F. J. Vecchio[1] and A. DeRoo[2]

ABSTRACT: Concrete tension splitting mechanisms can contribute measurably to the dilatation of cracked reinforced-concrete elements, in some cases significantly affecting response. Analytical models based on the popular smeared-crack concept currently make no attempt to account for this action. Test data from reinforced-concrete panels subjected to uniaxial tension are examined. It is found that the lateral dilatation occurs at a rate roughly proportional to the incremental strains in the longitudinal (loaded) direction. Various possible influencing factors are studied, and a preliminary model is formulated. The model is incorporated into a nonlinear finite-element algorithm, providing reasonably accurate simulations of the responses observed. The correlations obtained indicate that further research in this area may be worth pursuing.

INTRODUCTION

Smeared-crack models have became prevalent for representing the behavior of reinforced-concrete membrane-type structures. These models tend to be conceptually and computational quite simple, yet are very effective in capturing essential behavior mechanisms in cracked reinforced concrete. Equilibrium, compatibility, and constitutive response are considered in terms of average stresses and average strains, although in some models consideration is given to local conditions at crack surfaces. Mechanisms relating to the deterioration in compression response due to transverse cracking, the influence of postcracking tensile stresses in the concrete, and the shear stresses on crack surfaces are most often included. A number of alternative formulations have been proposed, many of which have been incorporated into nonlinear finite-element algorithms [e.g., Cervenka and Pukl (1992), Hu and Schnobrich (1990), and Vecchio (1990)]. They have been shown to be sufficiently accurate in modeling response under a wide range of structural details and loading conditions.

Some anomalies have been observed, however, when smeared-crack analyses are made of elements loaded primarily in tension or combined tension and shear. This is particularly true in elements containing little or no transverse reinforcement (i.e., uniaxially reinforced). In such cases, the concrete tends to exhibit a postcracking dilatation effect that isn't properly accounted for in the smeared-crack models available. (See Fig. 1 for panel nomenclature.)

Consider panel PB14, tested by Bhide and Collins (1989), shown in Fig. 2(a). The panel contained no transverse reinforcement and was subjected to combined shear and uniaxial tension. After cracking, the panel resisted additional load by the formation of concrete struts tied by the longitudinal reinforcing bars and equilibrated by shear stresses on the crack surfaces. One would expect compressive strains to be measured in the direction of the compression struts, as would be predicted by smeared-crack models. Shown in Fig. 3(a) is the observed average straining in the principal compression direction (i.e., in the direction of the struts). Note that immediately after cracking, the average strains in the strut direction begin to increase and eventually become positive (i.e., tensile). The modified compression field theory (MCFT)

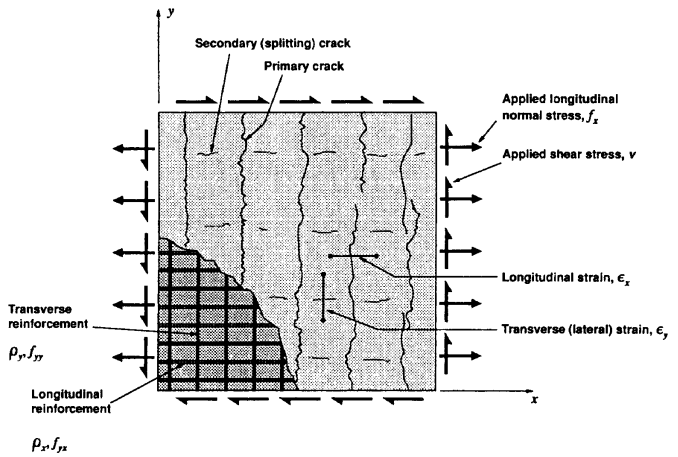

FIG. 1. Panel Subjected to Uniform Edge Loads

(Vecchio and Collins 1986) and other smeared-crack models would incorrectly predict continued compressive straining.

A more explicit demonstration of the problem can be seen in a panel tested in pure uniaxial tension. Panel PB13 (Bhide and Collins 1989), shown in Fig. 2(b), was uniaxially reinforced and subjected to direct tension in the direction of the reinforcement. Shown in Fig. 3(b) is the straining measured in the transverse direction. Prior to cracking at a stress of f_x = 1.5 MPa, the transverse strains were negative, as would be expected in consideration of Poisson's effect. After cracking, however, the transverse strains reversed direction and eventually attained significantly high positive values. After yielding of the longitudinal reinforcement at a load level of 4.35 MPa, the positive transverse straining effect accelerated. Most smeared-crack models assume no Poisson's effect after cracking, and thus would predict zero transverse strains in the postcracking load stages.

The dilatation effect observed in these and other panels is likely related to concrete tension-splitting action (i.e., the formation of splitting cracks in the concrete along the longitudinal reinforcing bars due primarily to the prying action of the deformations on the bars). As the example test specimens have demonstrated, the splitting action may significantly influence particular aspects of an element's load-deformation response under certain conditions. It may also be significant in cases where confinement is provided; for example, in the walls of offshore structures where out-of-plane reinforcement is typically used to help resist high punching shears. Concrete tension splitting action is unaccounted for in all current smeared crack models available.

This paper provides an initial investigation of the tension-splitting mechanism in the context of smeared-crack models for concrete, possibly pointing to the need for additional research. Evidence of postcracking concrete dilatation will be

[1]Prof., Dept. of Civ. Engrg., Univ. of Toronto, Toronto, Canada M5S 1A4.

[2]Engr., Evers Partners, Plein, The Netherlands.

Note. Associate Editor: Theodore Stathopoulos. Discussion open until November 1, 1995. To extend the closing date one month, a written request must be filed with the ASCE Manager of Journals. The manuscript for this paper was submitted for review and possible publication on January 12, 1994. This paper is part of the ***Journal of Engineering Mechanics***, Vol. 121, No. 6, June, 1995. ©ASCE, ISSN 0733-9399/95/0006-0702–0708/$2.00 + $.25 per page. Paper No. 7626.

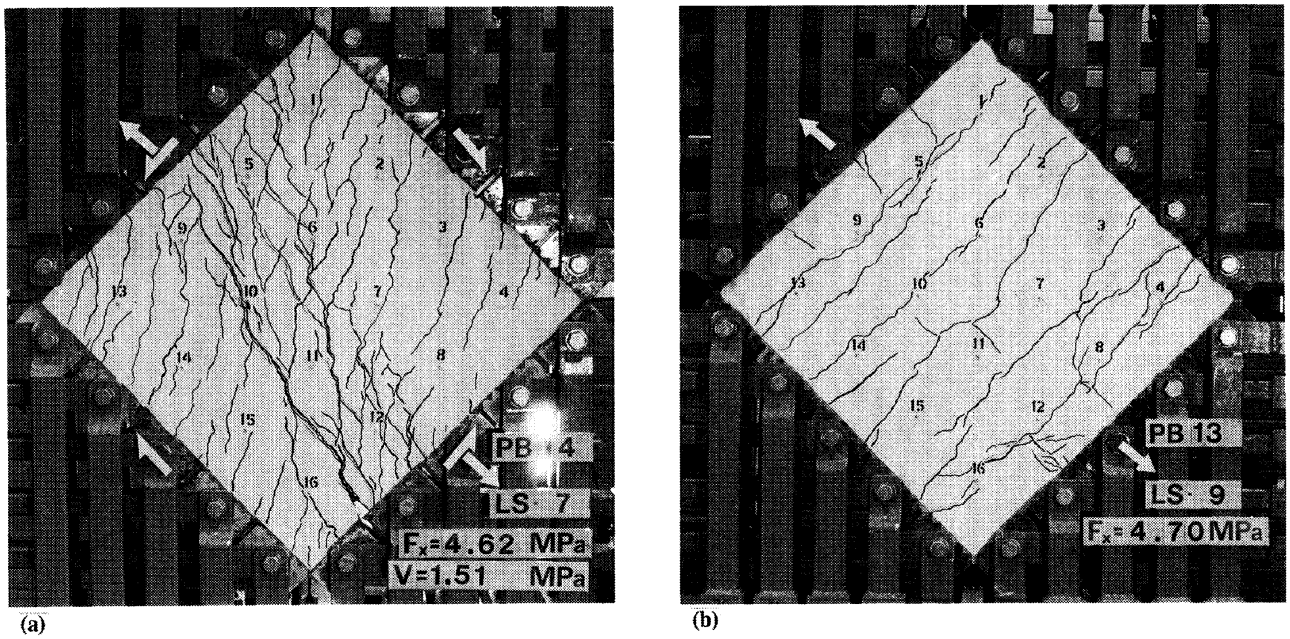

(a) (b)

FIG. 2. Test Panels: (a) PB14; (b) PB13

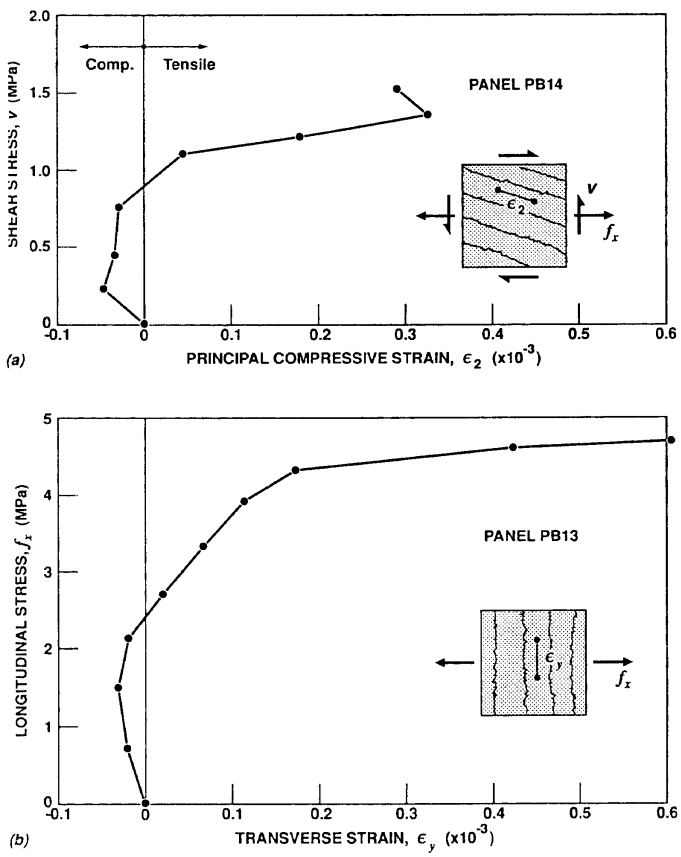

FIG. 3. Measured Response of Test Panels: (a) Strain in Compressive Strut Direction in PB14; (b) Lateral Strain in PB13

sought from test data available in the literature. A study will be made of behavior patterns and possible influencing factors, and a preliminary model will be formulated. The model will be incorporated into an existing nonlinear finite-element–analysis algorithm, and its influence on the computed response of concrete elements will be addressed.

TEST SPECIMENS

A number of reinforced-concrete panel specimens have been tested by several researchers under various loading conditions and using various apparatuses. Those panels that were initially subjected to uniaxial tension loading will be considered.

Bhide and Collins (1989) tested a large series of concrete panels under conditions of combined tension and shear; seven panels were fully or partially loaded in uniaxial tension first. They are identified as the PB-series specimens in Table 1, where corresponding material properties and reinforcement details are also given. Note that only two of the panels had transverse reinforcement (i.e., PB1 and PB2); the others were uniaxially reinforced. All the panels were loaded in tension to load stages well beyond yielding of the longitudinal reinforcement. Coglon (internal file notes, 1987) tested six panels, one of which was loaded in uniaxial tension (see PRC2, Table 1). Kollegger and Mehlhorn (1990) tested eight panels, two of which were initially loaded in tension (see PK3 and PK5, Table 1). The PB-, PRC-, and PK-series specimens were all tested at the University of Toronto, using the Shear Rig test facility shown in Fig. 4(a) [see Vecchio and Collins (1986) for details]. In all cases, the panels were 890 × 890 × 70 mm in dimension, and had nominal concrete strengths of about 25 MPa.

Kuchma (internal file notes, 1991) used the Shell Element Tester at the University of Toronto, shown in Fig. 4(b), to test a number of large-scale panels under various combinations of in-plane normal forces and shear. Two of these panels were initially subjected to uniaxial tension (see EZ2 and EZ3, Table 1). Belarbi and Hsu (1991) have also tested a large number of specimens in an ongoing research program at the University of Houston. Thirteen of the panels were initially loaded in uniaxial tension; these are represented in Table 1 as the E-series and R-series panels. Note that these specimens were relatively large-scale, with large-diameter reinforcing bars. Note too that the nominal concrete strength of these panels was substantially higher at around 40 MPa. The EZ-, E-, and R-series panels were subjected to changing load conditions with uniaxial tension representing only the initial

TABLE 1. Specimen Properties

Panel (1)	Dimensions (mm) (2)	Concrete		Longitudinal Reinforcement				Transverse Reinforcement			
		f'_c (MPa) (3)	ε_0 ($\times 10^{-3}$) (4)	ρ_x (%) (5)	f_{yx} (MPa) (6)	ϕ_b (mm) (7)	s_x (mm) (8)	ρ_y (%) (9)	f_{yy} (MPa) (10)	ϕ_b (mm) (11)	s_y (mm) (12)
PB1	890 × 890 × 70	28.1	1.72	1.30	234	5.4	51	1.30	234	5.4	51
PB2	890 × 890 × 70	23.0	1.90	1.99	240	4.8	25	1.99	243	4.8	25
PB13	890 × 890 × 70	23.4	1.81	1.08	414	6.6	89	0	—	—	—
PB24	890 × 890 × 70	20.4	1.98	1.10	407	6.6	89	0	—	—	—
PB25	890 × 890 × 70	20.6	1.98	2.20	414	6.6	45	0	—	—	—
PB26	890 × 890 × 70	22.6	2.13	1.01	502	6.3	89	0	—	—	—
PB27	890 × 890 × 70	37.9	3.15	2.02	502	6.6	45	0	—	—	—
PRC2	890 × 890 × 70	24.4	2.25	0.91	345	6.0	89	0.91	345	6.0	89
PK3	890 × 890 × 70	19.4	2.20	1.06	675	6.5	89	1.06	675	6.5	89
PK5	890 × 890 × 70	17.3	2.10	1.06	675	6.5	89	1.06	675	6.5	89
EZ2	1,625 × 1,625 × 205	31.2	2.22	1.70	932	16.0	102	0.64	452	11.3	152
EZ3	1,625 × 1,625 × 238	41.0	2.00	1.47	932	16.0	102	0.55	452	11.3	152
E1.5-1	1,400 × 1,400 × 178	44.6	2.10	1.20	448	19.1	267	0.54	544	12.7	267
E1.5-1B	1,400 × 1,400 × 178	39.0	2.30	1.20	521	9.5	67	0.54	498	12.7	267
E2-1	1,400 × 1,400 × 178	47.7	2.25	1.20	448	19.1	267	0.54	544	12.7	267
E2′-1	1,400 × 1,400 × 178	39.6	2.10	1.20	495	19.1	267	0.54	498	12.7	267
E2-1A	1,400 × 1,400 × 178	44.9	2.10	1.09	544	12.7	134	0.54	544	12.7	267
E2-1B	1,400 × 1,400 × 178	38.3	2.20	1.20	521	9.5	67	0.54	498	12.7	267
E4-1	1,400 × 1,400 × 178	40.6	2.05	1.20	495	19.1	267	0.54	498	12.7	267
E4-0.5	1,400 × 1,400 × 178	39.2	2.40	0.54	498	12.7	267	0.54	498	12.7	267
E4.2	1,400 × 1,400 × 178	37.0	2.35	2.10	469	25.2	267	0.54	498	12.7	267
E4-1A	1,400 × 1,400 × 178	37.3	2.30	1.09	498	12.7	134	0.54	498	12.7	267
E10-1A	1,400 × 1,400 × 178	36.9	2.15	1.69	462	16.0	134	0.54	498	12.7	267
E10-1B	1,400 × 1,400 × 178	39.6	2.40	1.69	466	11.2	67	0.54	498	12.7	267
R10-1	1,400 × 1,400 × 178	39.1	2.30	1.27	447	19.5	267	0.54	498	12.7	267

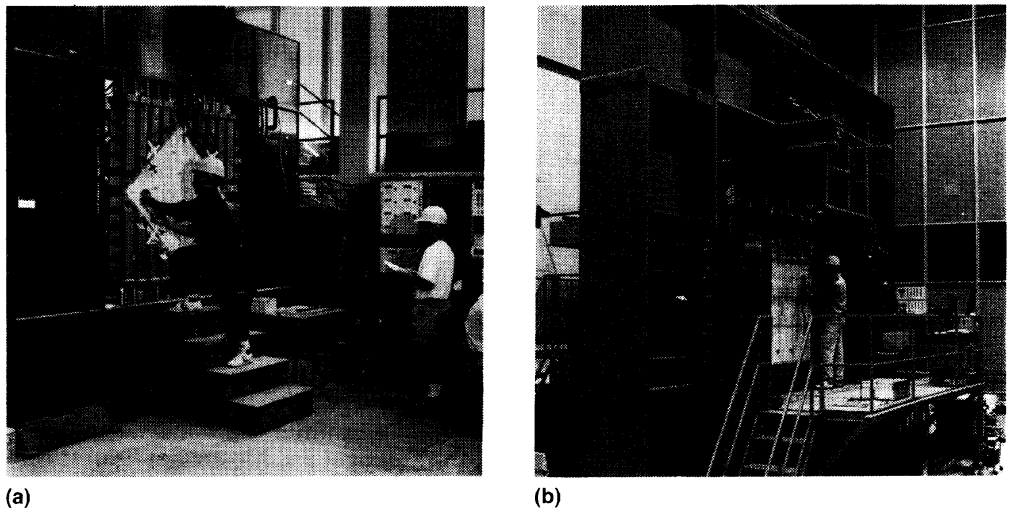

(a) (b)

FIG. 4. Test Facilities: (a) Shear Rig; (b) Shell Element Tester

condition. In all cases, the loading was changed before yielding of the longitudinal reinforcement was achieved.

Regular deformed reinforcement bars were used in all of the panels noted previously, typically provided in two layers in each direction. The nominal clear cover to the longitudinal reinforcement (i.e., outer layer) was approximately 6 mm for the PB-, PRC-, and PK-panels. In the larger panels, the cover ranged from 15 mm (EZ2) to 30 mm (EZ3).

Loads were applied in a monotonically increasing manner. At discrete load stages, loading was held constant temporarily as measurements and readings were taken. Specimen strains were measured using mechanical strain gauges on the concrete surfaces, continuously monitored linear variable differential transducers (LVDTs), and electrical strain gauges applied to the reinforcing bars. The mechanical-gauge target points were typically applied in a 200-mm grid pattern on both surfaces of the test specimens. The readings from the mechanical gauges were used for the data analyses that follow, except for the EZ-series, in which LVDT readings were used.

OBSERVED DILATATION RESPONSE

The test panels showed similar trends in dilatation response, although there was considerable scatter in the magnitudes observed. The typical aspects of the response observed will be identified by examining panel PB13.

Shown in Fig. 5(a) are the average longitudinal strains (ε_x) and transverse strains (ε_y) measured on panel PB13 as the applied longitudinal stress (f_x) was increased. In the initial stages prior to cracking, the behavior observed was one expected from an elastic material. Negative strains developed in the transverse direction due to the usual Poisson's effect. Immediately after cracking of the panel at $f_x = 1.5$ MPa, however, the incremental lateral strains changed from negative (contraction) to positive (expansion). (The sudden re-

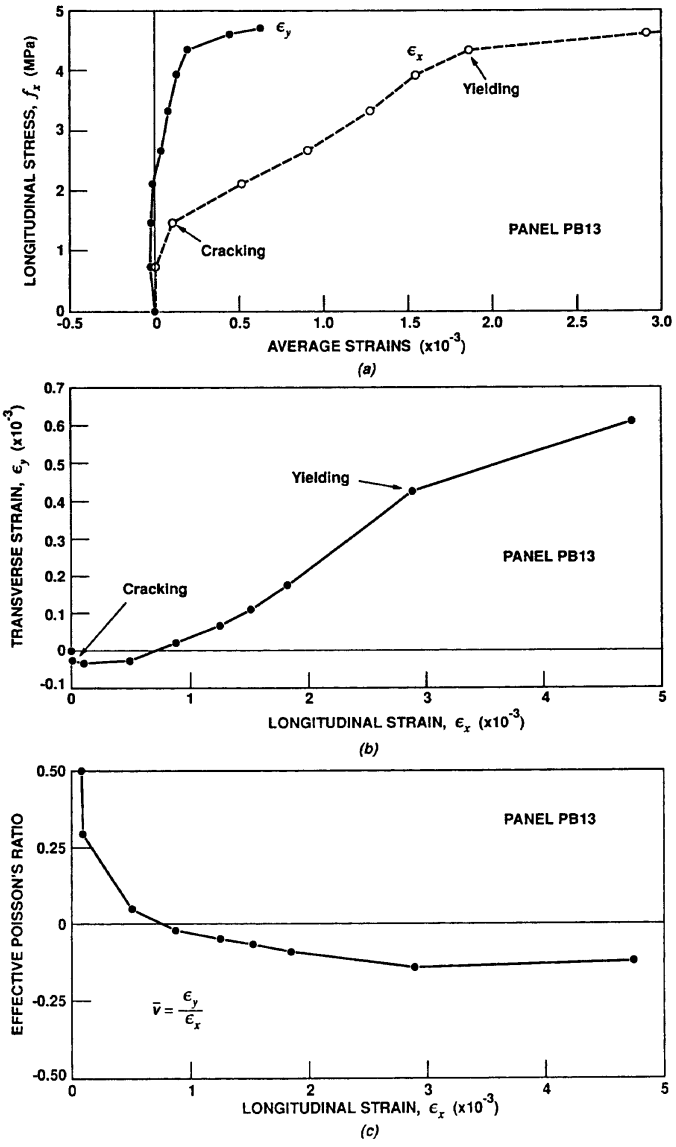

FIG. 5. Response of Panel PB13: (a) Longitudinal and Transverse Strains; (b) Correlation between Longitudinal and Transverse Strains; (c) Effective Postcracking Poisson's Ratio

versal in the lateral strains occurred immediately after longitudinal cracking, indicative of a tension-splitting mechanism, and was observed in all the panels investigated.) The dilatation of the panel continued in a regular manner as the load approached and then exceeded the yield load at $f_x = 4.5$ MPa. The rate of change in the transverse strains remained in a roughly fixed proportion to the changes in the longitudinal strains [see Fig. 5(b)]. A secant value for the effective Poisson's ratio can be determined by dividing the total transverse strain by the total longitudinal strain; the effective values at various stages of loading for PB13 are shown in Fig. 5(c). In the initial stages, prior to cracking, the effective Poisson's ratio is positive at about 0.25. In this range, however, accuracy is not good given the extremely small magnitudes of the strains measured. After cracking, the Poisson's ratio asymptotically approaches a value of about -0.15. This behavior seems unaffected by the progression from preyielding to postyielding response.

The secant value of the effective Poisson's ratio calculated for the remaining test panels, at the various stages of loading, are given in Fig. 6. Virtually all the specimens exhibited a pronounced lateral dilatation commencing shortly after cracking. Also apparent, however, is that the magnitude of this effect varied considerably from specimen to specimen.

ANALYSIS OF TEST DATA

The roughly constant proportional relation between the changes in the transverse strain and longitudinal strain, observed in most of the specimens, prompted a more detailed examination. Incremental (tangent) values for the effective Poisson's ratio, from one load stage to the next, were determined for each specimen. Corrections for the confining effect of transverse reinforcement, for those panels so reinforced, were made. Thus, the incremental Poisson's ratio ($\dot{\nu}$) was calculated as follows:

$$\dot{\nu} = -\frac{\dot{\epsilon}_y}{\dot{\epsilon}_x} \cdot \frac{1}{(1 + \rho_y \cdot n)} \tag{1}$$

where $\dot{\epsilon}_y$ = increment in transverse strain; $\dot{\epsilon}_x$ = increment in longitudinal strain; ρ_y = transverse reinforcement ratio; and n = modular ratio ($n = E_s/E_c$).

Prior to cracking, the lateral behavior was governed by the usual Poisson's effect. The small strains measured in this stage of loading made numerical study difficult. However, it appeared that the Poisson's ratio was relatively constant for each specimen, and had a value in the range of 0.15–0.25.

In the load stages between cracking and yielding of the panels, the effective dilatation observed was characterized by a near-constant negative-value incremental Poisson's ratio. In other words, the plot of the transverse strain versus the longitudinal strain typically followed a quasi-straight line with a positive slope [as seen, for example, in Fig. 5(b) for panel PB13]. The average incremental Poisson's ratios determined for each of the test panels are given in Table 2. The negative of the postcracking incremental Poisson's rate will henceforth be referred to as the dilatation factor.

The postyielding dilatation effect observed in the test panels was also examined. This was done for the PB- and PRC-panels only, because all the other panels were not loaded up to their yield capacity. Again, an essentially constant proportion was found between the incremental lateral strains and the incremental longitudinal strains. The effective Poisson's ratios determined accordingly are given in Table 2.

In examining the postcracking, preyielding dilatation factors summarized in Table 2, several observations can be made. For the PB-, PRC-, and PK-series panels, the dilatation factor appeared to have a wide range of scatter, but the values were significantly influenced by the presence of transverse reinforcement. For the five panels having no transverse reinforcement (PB13, PB24, PB25, PB26, and PB27), the dilatation factor had an average value of 0.149. With the five 70-mm-thick panels that were transversely reinforced (PB1, PB2, PRC2, PK3, and PK5), the average dilatation factor was considerably lower at 0.074. Considering the much larger EZ- and E-series panels, all transversely reinforced, the dilatation factor was somewhat lower at 0.049. (Data for panels E4-0.5, E10-1B, and R10-1 were too erratic to be considered reliable, and thus were not included.)

The postyielding dilatation response showed similar behavior. For the five PB-panels having no transverse reinforcement, the postyielding dilatation factor had a mean value of 0.206. This is greater than the corresponding preyield value of 0.149, but is influenced by a suspiciously high value recorded for PB27. Otherwise, the mean preyield and postyield values are nearly identical. For the three panels that were transversely reinforced and loaded beyond yield, the mean postyield dilatation factor was 0.071; again, very similar to the mean preyield value of 0.074.

Several trends appear to have emerged from the data. First,

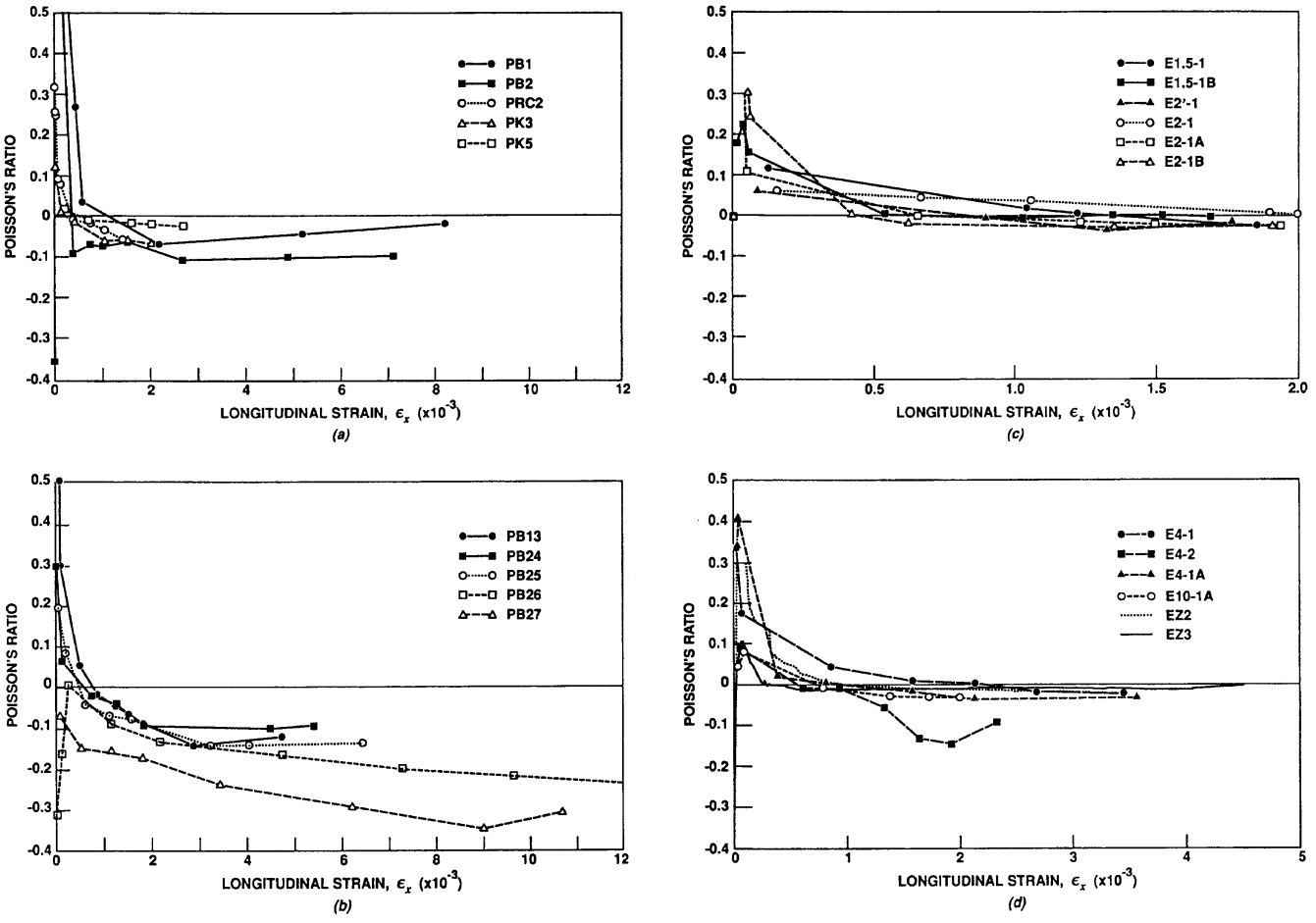

FIG. 6. Postcracking Dilatation Observed in Test Panels, Represented as Effective Poisson's Ratio (Secant Value)

TABLE 2. Incremental Poisson's Ratio

PREYIELDING						POSTYIELDING			
Group 1		Group 2		Group 3		Group 4		Group 5	
Panel (1)	$\dot{\nu}$ (2)	Panel (1)	$\dot{\nu}$ (2)	Panel (1)	$\dot{\nu}$ (2)	Panel (1)	$\dot{\nu}$ (2)	Panel (1)	$\dot{\nu}$ (2)
PB1	−0.106	PB13	−0.146	EZ2	−0.030	PB1	−0.005	PB13	−0.100
PB2	−0.088	PB24	−0.109	EZ3	−0.014	PB2	−0.094	PB24	−0.101
PRC2	−0.071	PB25	−0.156	E1.5-1	−0.085	PRC2	−0.114	PB25	−0.133
PK3	−0.076	PB26	−0.155	E1.5-1B	−0.017			PB26	−0.276
PK5	−0.029	PB27	−0.178	E2-1	−0.047			PB27	−0.420[a]
				E2'-1	−0.047				
				E2-1A	−0.030				
				E2-1B	−0.038				
				E4-1	−0.040				
				E4-2	−0.151				
				E4-1A	−0.047				
				E10-1A	−0.036				
Average	−0.074	—	−0.149	—	−0.049	—	−0.071	—	−0.153

[a]Suspect: excluded.

the rate of postcracking lateral expansion of transversely reinforced panels (i.e., group-1 and group-3 panels, Table 2), accompanying the longitudinal straining due to uniaxial tensile loading, remains relatively constant at a value of about 0.06. The dilatation rate appears to be insensitive to yielding of the longitudinal reinforcement (compare group 1 to group 4 and group 2 to group 5, Table 2). Second, the rate of dilatation appears to be significantly greater in panels containing no transverse reinforcement (group-2 panels, Table 2). (Transverse reinforcement, of course, plays an effective role in controlling tension-splitting cracks.) Finally, the smaller panels exhibited somewhat greater rates of dilatation than did the larger panels (group-1 versus group-3 panels, Table 2). Apart from size, the two groups of panels also differed significantly in the nominal strengths of the concrete. It is not possible to say which of the two factors contributed more to the difference in response noted between the two groups of panels.

A number of other parameters were investigated for possible influence on the nature and magnitude of the dilatation response observed in the test panels. These included percentage of longitudinal reinforcement, percentage of transverse reinforcement, bar size and spacing, cover, and concrete strength. The data base was insufficient to identify any strong influences from these factors.

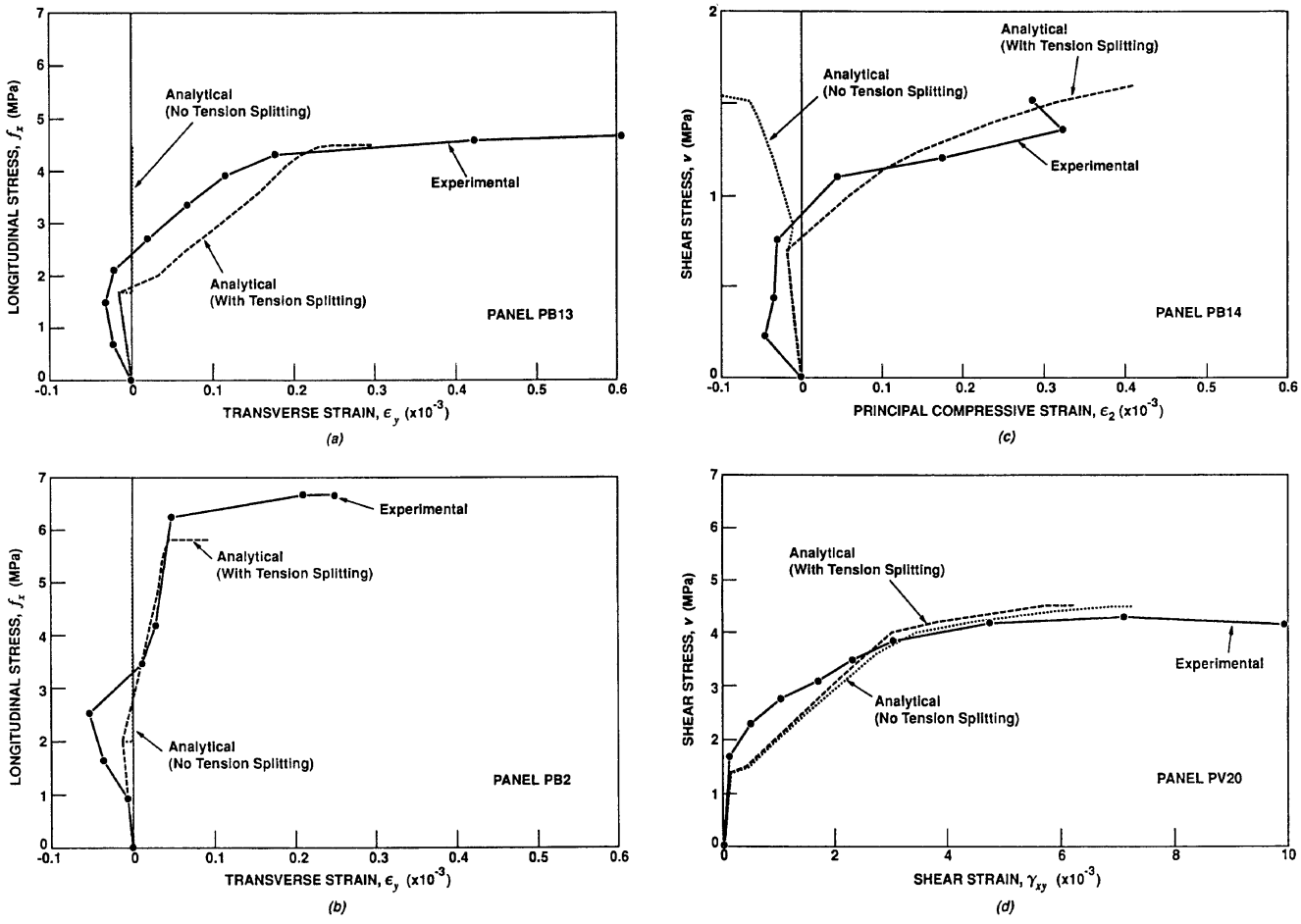

FIG. 7. Correlation between Experimental and Analytical Responses: (a) PB13; (b) PB2; (c) PB14; (d) PV20

FINITE-ELEMENT MODELING

The dilatation effects described previously, arising from tension-splitting action, can be incorporated into finite-element analysis routines by using a modified Poisson's ratio $\dot{\nu}_{21}$. (The ratio $\dot{\nu}_{21}$ represents strains in the principal compressive direction due to actions in the principal tensile direction.) Thus, for cracked reinforced concrete in a tension-compression state (i.e., $\varepsilon_1 > \varepsilon_{cr}$), the following effective Poisson's ratio is suggested:

$$\dot{\nu}_{21} = -0.06 \quad \text{when} \quad \rho_2 > 0 \tag{2a}$$

$$\dot{\nu}_{21} = -0.15 \quad \text{when} \quad \rho_2 = 0 \tag{2b}$$

The negative values denote directions opposite to the usual sense in a customary Poisson's effect. In a secant stiffness formulation, the modified Poisson's ratio would be as follows:

$$\bar{\nu}_{21} = \frac{\dot{\nu}_{21} \cdot (\varepsilon_1 - \varepsilon_{cr}) + \nu_0 \cdot \varepsilon_{cr}}{\varepsilon_1} \tag{3}$$

where ν_0 = initial (precracking) value, which can be taken at 0.15.

The foregoing model was incorporated into the nonlinear finite-element program TRIX [see Vecchio (1990)]. The algorithm employed is based on a total-load, secant stiffness formulation. Nonsymmetric stiffness matrices are avoided by using the prestrain technique, described by Vecchio (1992), to model all concrete expansions including those associated with Poisson's effects.

The modified finite-element program was used to analyze several panels. Among those examined were PB13, a uniaxially reinforced panel loaded in uniaxial tension (see Table 1); PB2, a biaxially reinforced panel loaded in uniaxial tension (see Table 1); PB14, a uniaxially reinforced panel subjected to combined uniaxial tension and shear in the proportion $f_x:f_y:v = 3.0:0:1$ (Bhide and Collins 1989); and PV20, a biaxially reinforced panel loaded in pure shear (Vecchio and Collins 1986). Comparisons of the predicted and observed responses are made in Fig. 7. Also shown are the calculated responses that would otherwise be obtained if the tension splitting model were omitted.

With the two panels loaded in uniaxial tension, the tension-splitting model implemented does much to account for the dilatations observed normal to the direction of loading. The pattern and magnitude of the postcracking expansions are modeled reasonably accurately [see Figs. 7(a and b)]. Omitting the tension-splitting model would result in predictions of zero transverse strains after initial cracking. Other aspects of behavior, such as load-deformation response in the direction of loading, are unaffected.

The tension-splitting model is seen to exert a major influence on the calculated response of the uniaxially reinforced panel subjected to tension and shear (PB14) [see Fig. 7(c)]. The strains in the principal compressive direction become tensile immediately after cracking of the panel and achieve significantly high levels. The pattern of the calculated response correlates to the experimentally measured response reasonably well, allowing for the fact that the measured and predicted cracking stress of the concrete differed significantly. As also seen in Fig. 7(c), ignoring the dilatation effect in the analytical model results in predictions of increasing compressive strain in the strut direction. With the biaxially reinforced panel loaded in pure shear (PV20), consideration of the dilatation effects give rise to a slight stiffening of the panel

as the concrete expansion is resisted by the reinforcement. The result is a marginally stiffer shear deformation response in the intermediate load stages, compared to what is otherwise obtained if the tension splitting model is not considered [see Fig. 7(d)]. Accuracy, relative to the measured response, is not measurably improved however. The calculated ultimate load capacity, stresses in the reinforcement, and stresses in the concrete are insignificantly affected.

CONCLUSIONS

The experimental evidence available clearly points to a systematic occurrence of lateral postcracking dilatation in panels subjected to uniaxial tension. The behavior is likely derived from concrete tension splitting actions, manifested by secondary cracks developing in-line with deformed longitudinal reinforcing bars. The concrete element's load-deformation behavior is, in some cases, significantly affected. Current smeared-crack models make no attempt to account for this behavior.

The test data examined indicate some possibly consistent trends in the dilatation response. After cracking, the dilatation in the lateral direction increases at a rate in roughly fixed proportion to the incremental strains in the longitudinal direction. This rate is not significantly affected by the onset of yielding of the longitudinal reinforcement. The rate is substantially higher in elements containing no transverse reinforcement, however. The dilatation rate may also be related to size factors and/or concrete strength.

The dilatation behavior can be simulated by defining an effective postcracking Poisson's ratio. A preliminary value for the ratio is -0.06; the negative value is indicative of a direction opposite in sense to that usually associated with a Poisson's effect. In this manner, the dilatation effect can easily be incorporated into finite-element algorithms and reasonably accurate simulations can be achieved.

The experimental data and the analysis results reported are sufficiently strong to suggest that a smeared-crack representation of tension splitting is both possible and potentially useful. A more comprehensive experimental investigation is required to better quantify the behavior, and to address the influence of such factors as longitudinal reinforcement ratio, transverse reinforcement ratio, bar size and spacing, cover, and concrete strength. The behavior must also be examined under conditions in which the principal tensile loading is in a skew direction to the reinforcement.

APPENDIX I. REFERENCES

Belarbi, A., and Hsu, T. T. C. (1991). "Constitutive laws of reinforced concrete in biaxial tension-compression." *Res. Rep. UHCEE 91-2*, Univ. of Houston, Houston, Tex.

Bhide, S. B., and Collins, M. P. (1989). "Influence of axial tension on the shear capacity of reinforced concrete members." *ACI Struct. J.*, 86(5), 570–581.

Cervenka, V., and Pukl, R. (1992). "Computer models of concrete structures." *IABSE Struct. Engrg. Int.*, Vol. 2, 103–107.

Hu, H. T., and Schnobrich, W. C. (1990). "Nonlinear analysis of cracked reinforced concrete." *ACI Struct. J.*, 87(2), 199–207.

Kollegger, J., and Mehlhorn, G. (1990). "Experimentelle Untersuchungen zur Bestimmung der Druckfestigkeit des gerissenen Stalhbetons bei einer Querzugbeanspruchung." *Rep. 413*, Deutscher Ausschuss Fur Stahlbeton, Berlin, Germany (in German).

Vecchio, F. J. (1990). "Reinforced concrete membrane element formulations." *J. Struct. Engrg.*, ASCE, 116(3), 730–750.

Vecchio, F. J. (1992). "Finite element modelling of concrete expansion and confinement." *J. Struct. Engrg.*, ASCE, 118(9), 2390–2406.

Vecchio, F. J., and Collins, M. P. (1986). "The modified compression field theory for reinforced concrete elements subjected to shear." *ACI J.*, 83(2), 219–231.

APPENDIX II. NOTATION

The following symbols are used in this paper:

E_c = modulus of elasticity of concrete;
E_s = modulus of elasticity of reinforcing steel;
f'_c = concrete cylinder 28-day compressive strength;
f_x = applied normal stress in longitudinal (x) direction;
f_{yx} = yield stress of x-direction reinforcement;
f_{yy} = yield stress of y-direction reinforcement;
n = modular ratio;
s_x = spacing of x-direction reinforcing bars;
s_y = spacing of y-direction reinforcing bars;
v = applied shear stress on panel;
γ_{xy} = average shear strain relative to x, y and axes;
ε_{cr} = cracking strain of concrete;
ε_0 = strain of concrete at peak cylinder stress;
ε_x = average strain in x-direction—longitudinal strain;
ε_y = average strain in y-direction—transverse strain;
ε_1 = average principal tensile strain in concrete;
ε_2 = average principal compressive strain in concrete;
$\dot{\nu}$ = postcracking Poisson's ratio—tangent value;
$\bar{\nu}$ = postcracking Poisson's ratio—secant value;
ν_0 = initial (precracking) Poisson's ratio;
ρ_x = longitudinal reinforcement ratio;
ρ_y = transverse reinforcement ratio;
ρ_2 = reinforcement ratio perpendicular to principal tensile strain direction; and
ϕ_b = bar diameter.